

## REPORT

## ANTIBIOTIC RESISTANCE

# Biased partitioning of the multidrug efflux pump AcrAB-TolC underlies long-lived phenotypic heterogeneity

Tobias Bergmiller,<sup>1\*</sup> Anna M. C. Andersson,<sup>1\*</sup> Kathrin Tomasek,<sup>1</sup> Enrique Balleza,<sup>2</sup> Daniel J. Kiviet,<sup>3</sup> Robert Hauschild,<sup>1</sup> Gašper Tkačik,<sup>1</sup> Čalín C. Guet<sup>1†</sup>

The molecular mechanisms underlying phenotypic variation in isogenic bacterial populations remain poorly understood. We report that AcrAB-TolC, the main multidrug efflux pump of *Escherichia coli*, exhibits a strong partitioning bias for old cell poles by a segregation mechanism that is mediated by ternary AcrAB-TolC complex formation. Mother cells inheriting old poles are phenotypically distinct and display increased drug efflux activity relative to daughters. Consequently, we find systematic and long-lived growth differences between mother and daughter cells in the presence of subinhibitory drug concentrations. A simple model for biased partitioning predicts a population structure of long-lived and highly heterogeneous phenotypes. This straightforward mechanism of generating sustained growth rate differences at subinhibitory antibiotic concentrations has implications for understanding the emergence of multidrug resistance in bacteria.

In bacteria, phenotypic heterogeneity arises through stochastic molecular processes in the cell. As a result, isogenic cells can exhibit distinct gene expression levels and phenotypes that fluctuate over time. Contributions of gene expression noise to phenotypic heterogeneity have been extensively studied (1), with qualitatively similar effects expected due to degradation (2) or random partitioning of cytosolic proteins at cell division (3). In contrast to cytosolic components, outer membrane proteins are diffusion-restricted due to the formation of supramolecular islands (4, 5) and thus violate the well-mixedness assumption. As a consequence, the outer membrane undergoes asymmetric turnover, which leads to polar localization of at least some outer membrane proteins (5, 6). In rod-shaped bacteria, the two sister cells emerging from cell division can be distinguished by the age of their poles: One sister cell is characterized by an old cell pole originating from a division event in the past. Old poles are considered inert with respect to envelope composition (5, 7), and, as a result, individual cells—and sister cells in particular—could exhibit systematic differences in envelope composition.

The bacterial envelope functions as a highly effective diffusive barrier (8). A key determinant of envelope permeability to toxic compounds is the multidrug efflux pump AcrAB-TolC (9, 10), a tripartite complex that bridges the entire cell envelope and allows transport of harmful chemicals directly to the outside medium (fig. S1) [see the supplementary materials (11)]. TolC interacts with several different excretion and secretion systems (12). However, AcrAB in complex with TolC is the main multidrug efflux determinant in *Escherichia coli* and enterobacteria (9, 13, 14). Here, we studied phenotypic heterogeneity as a result of polar cell envelope localization in *E. coli*. We monitored the partitioning dynamics of AcrAB-TolC over many generations and measured efflux activity and drug sensitivity of individual cells.

We tracked a chromosomally encoded functional AcrB-GFP (green fluorescent protein) (fig. S2) as a specific marker of AcrAB-TolC partitioning in single cells growing inside a microfluidic “mother machine” device (15). Mother cells, which are the sister cells characterized by an increasingly old cell pole, remain captured at the closed end of channels while undergoing cell divisions (Fig. 1A and fig. S3). Daughter cells are pushed toward the main trench by cell growth. *E. coli* cells exhibited stable and robust growth inside these microfluidic devices (15) (fig. S4 and table S1).

We found that AcrB-GFP accumulates at the old pole in mother cells (Fig. 1B, figs. S5 and S6, and movie S1) in a TolC-dependent manner, whereas deletion of *tolC* led to uniformly distributed AcrB-GFP in the inner membrane (Fig. 1C). As previously reported, deletion of *tolC* also causes increased *acrAB* expression (16). Polar AcrB-GFP

localization was restored by complementing TolC expression (fig. S7). When comparing the old and newly formed poles of mothers, we found that AcrB-GFP localization asymmetry increased slowly with the replicative age of the old cell pole (Fig. 1D). AcrB-GFP accumulated at old cell poles in general, as is visible in D3 daughters that carry the next oldest cell pole (Fig. 1D, right panel, and table S2). AcrB-GFP asymmetry was absent in  $\Delta tolC$  cells (Fig. 1D). Direct comparison of mother and daughter cells immediately before and after cell division showed an average of 58% AcrB-GFP retained in mother cells, corresponding with a  $16.0 \pm 0.3\%$  mother-daughter difference (Fig. 1E). In the absence of TolC, AcrB-GFP partitioned similar to cytosolic mCherry (Fig. 1E, right bar, and fig. S8). TolC-GFP also accumulated at old cell poles, with lesser magnitude and higher overall variability; its asymmetry was substantially reduced in the  $\Delta acrAB$  strain (fig. S9). Thus, only complete ternary AcrAB-TolC complexes are partitioned unequally at cell division.

To probe the lifetime of AcrB-GFP at the old cell pole of mothers, we transiently expressed AcrB-GFP (pulse) (Fig. 1F, fig. S10, and movie S2). AcrB-GFP asymmetry in mother cells was constant for several generations during the chase period and was ultimately followed by a slow decay in asymmetry. In contrast, soluble GFP showed no induction-dependent asymmetry. AcrB-GFP thus segregates with the old mother pole for an extended period even in the absence of *acrB-gfp* expression and is partitioned unevenly at cell division. Using total internal reflection fluorescence microscopy, we found that AcrB-GFP formed TolC-dependent stationary foci that segregated for prolonged time periods within individual cells (fig. S11). Taken together, our results suggest that ternary complexes are trapped and immobilized and thus segregate within individual cells for an extended time exceeding a typical cell lifetime, thereby enabling biased partitioning.

We next asked whether uneven partitioning of AcrAB-TolC translates into differences in efflux activity between mother and daughter cells. We assessed real-time efflux activity using the dye Hoechst (H) 33342, which becomes fluorescent when incorporated into bacterial cells (17). Mother cells displayed decreased dye uptake (which is a proxy for higher efflux activity) and contained significantly less dye than daughter cells at steady state; deletion of *tolC* abrogated this difference (Fig. 2A). Additionally, the amount of H33342 was anticorrelated with AcrB-GFP fluorescence in mother and daughter cells (Fig. 2B), which indicated that the amount of AcrB-GFP per individual cell is a proxy for single-cell efflux activity. AcrB-GFP had similar efflux activity to AcrB-only cells (fig. S12). Fluorescence-activated cell sorting experiments confirmed the association between AcrB-GFP and efflux activity, independent of microfluidic measurements (fig. S13).

Next, we used growth as a proxy for drug sensitivity of mother and daughter cells toward tetracycline, a bacteriostatic AcrAB-TolC substrate (13), which reduces growth rate at subinhibitory

<sup>1</sup>Institute of Science and Technology Austria, 3400 Klosterneuburg, Austria. <sup>2</sup>Faculty of Arts and Sciences, Center for Systems Biology and Department of Molecular and Cellular Biology, Harvard University, Cambridge, MA 02138, USA. <sup>3</sup>Department of Environmental System Science, ETH Zurich, Swiss Federal Institute of Technology, 8092 Zurich, Switzerland, and Department of Environmental Microbiology, Eawag, Swiss Federal Institute of Aquatic Science and Technology, 8600 Dübendorf, Switzerland. \*These authors contributed equally to this work. †Corresponding author. Email: calin@ist.ac.at

concentrations (18). To measure gradual differences in sensitivity, cells were exposed to intervals of stepwise increasing subinhibitory tetracycline concentrations, with the highest concentration representing the half-maximal inhibitory concentration ( $IC_{50}$ ). Increasing concentrations strongly affected growth of single cells in general: Elongation rate ( $\alpha$ ) decreased, and cell-cycle duration

( $T$ ) increased on average (Fig. 3A). Importantly, increasing tetracycline concentrations unveiled differences in sensitivity between mother and daughter cells: Daughter cells showed larger average changes in  $\alpha$  and  $T$ , increased variance in  $T$  (Fig. 3B), and hence unbalanced growth that deviates from exponential, thus effectively decoupling  $\alpha$  and  $T$  (fig. S14). These differences

were consistent across replicate experiments (table S3).

Analyzing differences in growth within individual mother-daughter pairs, we found that with increasing tetracycline concentration, mother cells grew faster and contained more AcrB-GFP (Fig. 3C). When cells were exposed to a single intermediate concentration of tetracycline, we measured

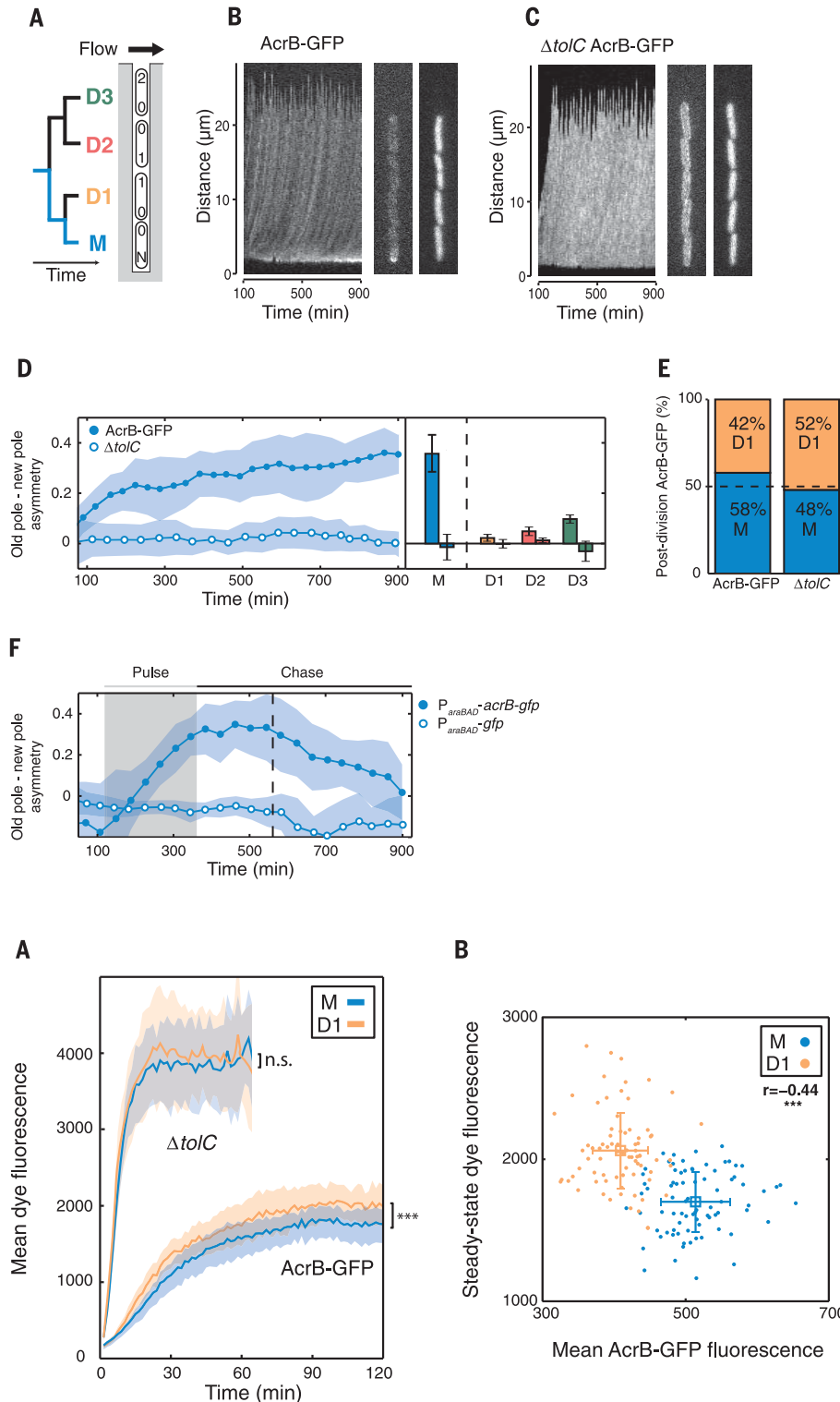


**Fig. 1. AcrB-GFP accumulates at old cell poles and undergoes biased partitioning.**

(A) Schematic representation of a mother machine growth channel. A mother cell M is captured at the channel closed end, repeatedly dividing into M and D1 (daughter) cells; a D1 cell divides into daughter cells D2 and D3. Numbers represent pole ages, and N represents the increasingly old mother cell pole. (B and C) Kymographs of wild-type and  $\Delta tolC$  strains expressing AcrB-GFP growing in mother machine. Snapshots of AcrB-GFP and soluble mCherry expressed within the same cells. (D) (Left) Within-cell fluorescence asymmetry in M cells expressing AcrB-GFP, quantified as (old cell half - new cell half)/(whole cell). Data are from 20 mother cells (~34 cell divisions each), smoothed over three time bins. Dots, mean generation times; envelope, SD over cells. (Right) Bar for M shows final asymmetry; bars for D1/D2/D3 are time averages throughout the entire experiment. [Left bars, AcrB-GFP; all nonzero at  $P < 10^{-4}$ ,  $t$  test,  $N = 20$  for M (last time point); 691 (D1), 671 (D2), and 655 (D3). Right bars,  $\Delta tolC$ ;  $N = 18$  for M (last time point); 427 (D1), 383 (D2), and 406 (D3). Error bars, mean  $\pm 1$  SD (see table S1)]. (E) Partitioning of AcrB-GFP mean cell fluorescence between M and D1 at cell division [M/D1 different with  $P < 10^{-10}$  at left and  $P < 0.002$  at right,  $t$  tests; data from (D);  $N = 691, 425$ , respectively]. (F) Within-cell asymmetry in M cells during pulse-chase of  $P_{araBAD}$ - $acrB$ - $gfp$  and soluble  $P_{araBAD}$ - $gfp$ . Gray shading, pulse period. Dashed line indicates time point when soluble GFP fluorescence becomes undetectable above background. Envelope, SD over cells (18 lineages for AcrB-GFP, 17 lineages for GFP).

**Fig. 2. Real-time single-cell efflux assays show differential efflux activity between mother and daughter cells.**

(A) Side-by-side comparison of uptake dynamics of dye H33342 in individual M and D1 cells in strain expressing AcrB-GFP and  $\Delta tolC$  strain (sampled every 90 s). Lines, average dye fluorescence; envelopes, SD over cells. Final saturation levels, averaged over the last five time points, differ significantly between M and D1 cells for AcrB-GFP ( $P < 10^{-5}$ ,  $t$  test, 20 lineages) but not for  $\Delta tolC$  (15 lineages). (B) AcrB-GFP and H33342 fluorescence of individual cells at steady state, averaged over last five time points, correlate significantly (Pearson correlation, data from two independent experiments;  $N = 159$  from 66 lineages).

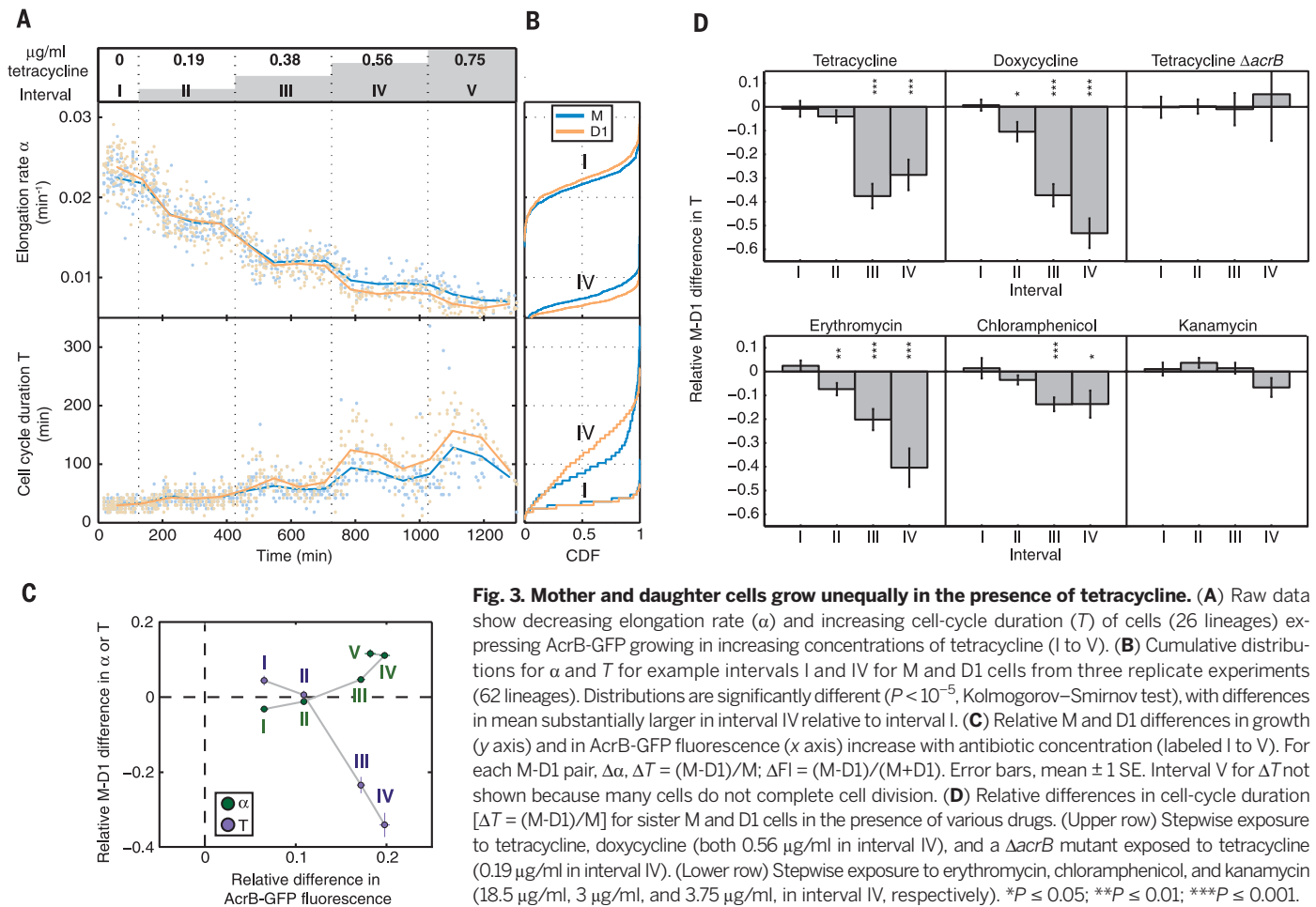


**Fig. 3. Mother and daughter cells grow unequally in the presence of tetracycline.** (A) Raw data show decreasing elongation rate ( $\alpha$ ) and increasing cell-cycle duration ( $T$ ) of cells (26 lineages) expressing AcrB-GFP growing in increasing concentrations of tetracycline (I to V). (B) Cumulative distributions for  $\alpha$  and  $T$  for example intervals I and IV for M and D1 cells from three replicate experiments (62 lineages). Distributions are significantly different ( $P < 10^{-5}$ , Kolmogorov–Smirnov test), with differences in mean substantially larger in interval IV relative to interval I. (C) Relative M and D1 differences in growth (y axis) and in AcrB-GFP fluorescence (x axis) increase with antibiotic concentration (labeled I to V). For each M-D1 pair,  $\Delta\alpha$ ,  $\Delta T = (M-D1)/M$ ;  $\Delta FI = (M-D1)/(M+D1)$ . Error bars, mean  $\pm 1$  SE. Interval V for  $\Delta T$  not shown because many cells do not complete cell division. (D) Relative differences in cell-cycle duration [ $\Delta T = (M-D1)/M$ ] for sister M and D1 cells in the presence of various drugs. (Upper row) Stepwise exposure to tetracycline, doxycycline (both 0.56  $\mu\text{g/ml}$  in interval IV), and a  $\Delta\text{acrB}$  mutant exposed to tetracycline (0.19  $\mu\text{g/ml}$  in interval IV). (Lower row) Stepwise exposure to erythromycin, chloramphenicol, and kanamycin (18.5  $\mu\text{g/ml}$ , 3  $\mu\text{g/ml}$ , and 3.75  $\mu\text{g/ml}$ , in interval IV, respectively). \* $P \leq 0.05$ ; \*\* $P \leq 0.01$ ; \*\*\* $P \leq 0.001$ .

qualitatively similar mother-daughter growth differences (fig. S15). This drug concentration-dependent growth advantage for mother cells was reversed and of smaller magnitude in a  $\Delta\text{acrB}$  strain, which had a lower  $\text{IC}_{50}$  ( $\sim 0.25$   $\mu\text{g/ml}$ ) (fig. S16A). A strain that carried  $\text{acrB}$  behaved similarly to the  $\text{acrB-gfp}$  strain (fig. S16B). Furthermore, differences in AcrB-GFP fluorescence and  $\alpha$  in individual mother-daughter pairs correlated within intervals III to V (fig. S17). When we tested ribosome-inhibiting antibiotics of different classes (tables S4 to S8), we found similar effects for all antibiotics that are substrates for AcrAB-TolC except for kanamycin, which served as a non-efflux control antibiotic:  $T$  was larger in D1 cells compared with their sister M cells at drug concentrations approaching  $\text{IC}_{50}$  (Fig. 3D and fig. S18).

We developed a stochastic nonequilibrium model of biased partitioning (Fig. 4A) to identify how its essential parameters affect population structure. Here, a gene is expressed at a rate of  $2\lambda$  per generation; half of the newly produced protein is inherited by each cell after division, whereas previously accumulated protein is partitioned in a binomial fashion with bias  $q$ . A  $q = 0.5$  corresponds to unbiased random partition, whereas for  $q > 0.5$  mother cells retain more AcrB-GFP than daughter cells. We extracted  $\lambda$  for each cell

cycle directly from AcrB-GFP fluorescence data and fitted  $q$  for every lineage. The inferred  $q^* = 0.62 \pm 0.01$  (Fig. 4B) indicated that partitioning is substantially biased toward mother cells, in line with direct experimental comparison of AcrB-GFP levels pre- and postdivision in mothers and daughters (Fig. 1E). In contrast, cytosolic mCherry expressed in the same cells (fig. S19) and AcrB-GFP in  $\Delta\text{tolC}$  cells were very close to  $q = 0.5$ .

This simple model captured two experimentally determined long-time scale features of AcrB-GFP data: the steady-state level and the time scale of accumulation in the mother cell (Fig. 4, C and D). Furthermore, our model made a parameter-free prediction for the AcrB-GFP decay time scale in the pulse-chase experiment in agreement with data (Fig. 4E). For random partition, the steady-state distribution of AcrAB-TolC across an exponentially growing population would be approximately Gaussian (Fig. 4F). As partitioning bias  $q$  increases, the distribution widens and develops a rightward skew with a growing overrepresentation of cells with high-efflux capacities (e.g., in our data, we expect about a sixfold enrichment of cells with efflux levels in the top 1% class relative to the unbiased partition expectation). This increase in population heterogeneity due to enrichment in extreme phenotypes is the first generic consequence of

biased partitioning predicted by our model. The second consequence is the emergence of a new time scale exceeding the generation time [by a factor of  $\log(0.5)/\log(q^*) \sim 1.4$  here] (Fig. 4, C and E) on which multidrug efflux phenotypes form, persist, and change. Importantly, biased partitioning generates long-lived heterogeneity without specialized regulatory mechanisms (19, 20).

Our experiments at subinhibitory antibiotic concentrations uncovered long-lived single-cell growth phenotypes that arise by biased partitioning of AcrAB-TolC. Recent work suggests that at low antibiotic concentrations, de novo resistance mutations can readily emerge on short time scales (18). Because selection can act on individual cell lineages in bacterial populations (21), small-effect mutations such as gene amplifications (22) might be specifically selected for in fast-growing lineages. Selection might be particularly strong in environments with low or fluctuating antibiotic concentrations, which increasingly occur in natural habitats as a result of human activity (23) and within patients during drug treatment (24). Notably, the  $\text{acrAB}$  locus was found to be amplified in low or intermediate antibiotic selection regimes (25), leading to high levels of efflux-based antibiotic resistance. Multi-drug efflux-mediated growth heterogeneity could

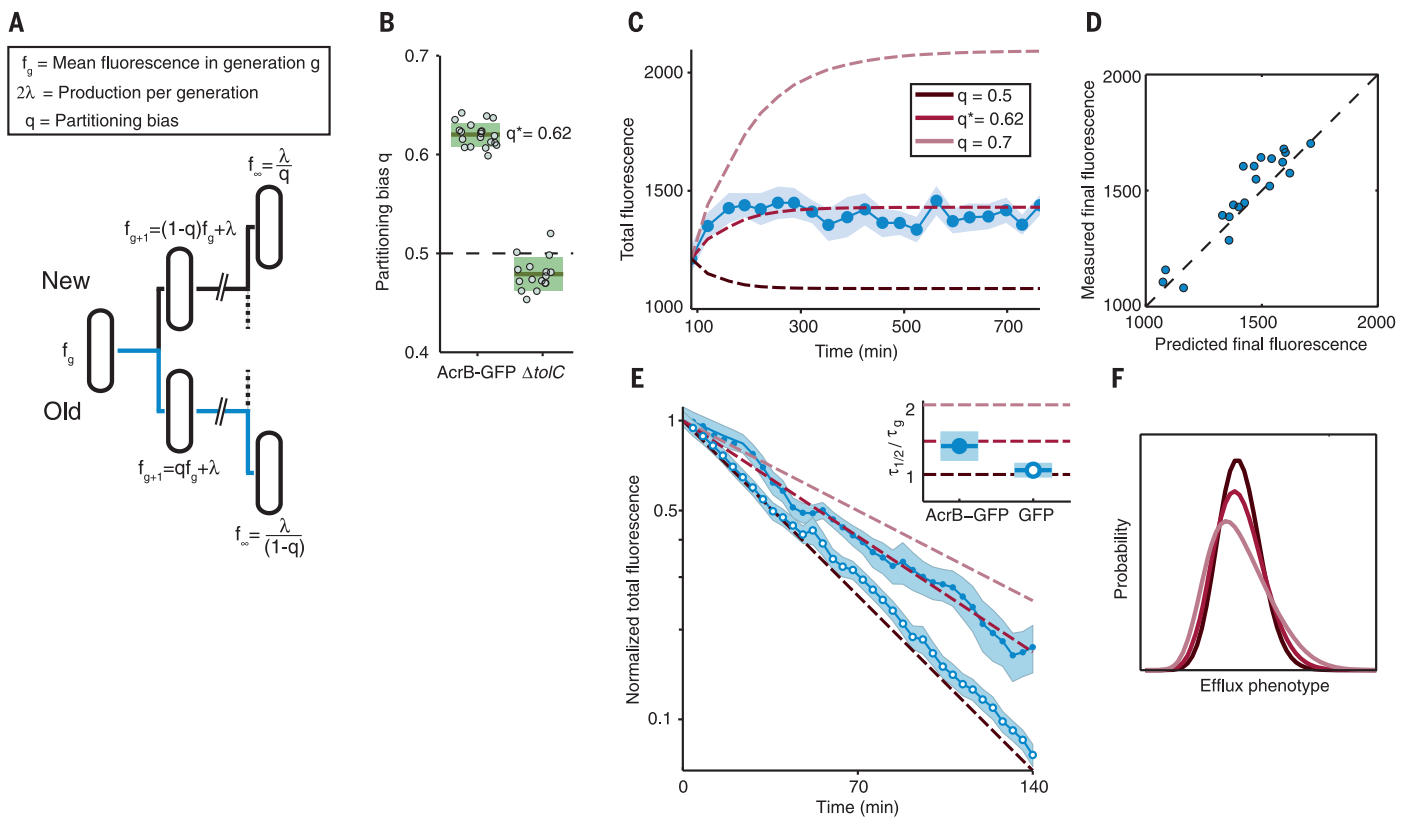


**Fig. 4. Model of biased partitioning predicts long accumulation time scale and large population heterogeneity.** (A) Model schematic: average fluorescence in generation  $(g + 1)$ ,  $f_{g+1}$ , is given by biased binomial partitioning (with bias  $q$ ) of fluorescence in generation  $g$ ,  $f_g$ , and symmetric partitioning of newly expressed protein, expressed at rate  $2\lambda$ . (B) Bias  $q$  for individual lineages (dots) in AcrB-GFP and  $\Delta tolC$ . Line and envelope, mean  $\pm$  SD over lineages. (C) Average AcrB-GFP fluorescence in mother cells (blue line, mean; envelope, mean  $\pm$  1 SE). Red, model prediction with  $q^*$  from (B); light red, hypothetical prediction for larger bias,  $q = 0.7$ ; dark red, prediction for symmetric partitioning,  $q = 0.5$ . (D) Measured

versus predicted steady-state AcrB-GFP fluorescence for individual lineages (dots), using  $q$  values from (B). (E) Decay of fluorescence in pulse-chase experiment from start of "chase" to dashed line of Fig. 1F (solid blue, AcrB-GFP; empty blue, cytosolic GFP) and parameter-free predictions using  $q^*$  for AcrB-GFP and  $q = 0.5$  for cytosolic GFP. Inset shows the match between the measured and predicted ratio of decay to generation time scale [ $t_g = T/\log(2)$ ], with  $T$  the mean doubling time). (F) Predicted steady-state distributions of efflux phenotypes in growing populations for three values of bias  $q$ ; increase in  $q$  beyond unbiased partitioning ( $q = 0.5$ ) leads to rightward skew.

serve as a stepping-stone on the path of bacterial populations toward antibiotic resistance.

#### REFERENCES AND NOTES

1. A. Sanchez, S. Choubey, J. Kondev, *Annu. Rev. Biophys.* **42**, 469–491 (2013).
2. N. A. Cookson et al., *Mol. Syst. Biol.* **7**, 561 (2011).
3. D. Huh, J. Paulsson, *Proc. Natl. Acad. Sci. U.S.A.* **108**, 15004–15009 (2011).
4. M. A. de Pedro, C. G. Grunfelder, H. Schwarz, *J. Bacteriol.* **186**, 2594–2602 (2004).
5. P. Rassam et al., *Nature* **523**, 333–336 (2015).
6. C. Kleanthous, P. Rassam, C. G. Baumann, *Curr. Opin. Struct. Biol.* **35**, 109–115 (2015).
7. J. Dworkin, *Cold Spring Harb. Perspect. Biol.* **1**, a003368 (2009).
8. T. J. Silhavy, D. Kahne, S. Walker, *Cold Spring Harb. Perspect. Biol.* **2**, a000414–a000414 (2010).
9. X.-Z. Li, P. Plésiat, H. Nikaïdo, *Clin. Microbiol. Rev.* **28**, 337–418 (2015).
10. D. Du et al., *Nature* **509**, 512–515 (2014).
11. Materials and methods are available as supplementary materials.
12. H. I. Zgurskaya, G. Krishnamoorthy, A. Ntresh, S. Lu, *Front. Microbiol.* **2**, 189 (2011).
13. M. C. Sulavik et al., *Antimicrob. Agents Chemother.* **45**, 1126–1136 (2001).
14. K. Nishino, A. Yamaguchi, *J. Bacteriol.* **183**, 5803–5812 (2001).
15. P. Wang et al., *Curr. Biol.* **20**, 1099–1103 (2010).
16. J. L. Rosner, R. G. Martin, *J. Bacteriol.* **191**, 5283–5292 (2009).
17. N. G. Coldham, M. Webber, M. J. Woodward, L. J. V. Piddock, *J. Antimicrob. Chemother.* **65**, 1655–1663 (2010).
18. E. Gullberg et al., *PLOS Pathog.* **7**, e1002158 (2011).
19. B. M. C. Martins, J. C. Locke, *Curr. Opin. Microbiol.* **24**, 104–112 (2015).
20. T. M. Norman, N. D. Lord, J. Paulsson, R. Losick, *Annu. Rev. Microbiol.* **69**, 381–403 (2015).
21. S. Leibler, E. Kussell, *Proc. Natl. Acad. Sci. U.S.A.* **107**, 13183–13188 (2010).
22. D. I. Andersson, D. Hughes, *Annu. Rev. Genet.* **43**, 167–195 (2009).
23. F. Baquero, J. L. Martínez, R. Cantón, *Curr. Opin. Biotechnol.* **19**, 260–265 (2008).
24. F. Baquero, M. C. Negri, *BioEssays* **19**, 731–736 (1997).
25. D. Laehnemann et al., *Genome Biol. Evol.* **6**, 1287–1301 (2014).

#### ACKNOWLEDGMENTS

We thank V. Denic, M. Pleska, D. Siekhaus, and B. Stern for in-depth comments on the manuscript; A. W. Murray, P. Cluzel, B. R. Levin, and J. M. Marko for helpful discussions; and members of the Guet laboratory for comments. G.T. acknowledges Austrian Science Fund (FWF) grant P28844. D.J.K. was supported by Swiss

National Science Foundation grant 31003A\_149267 to M. Ackermann. E.B. was supported by Consejo Nacional de Ciencia y Tecnología de México (CONACYT) and the Pew Foundation Latin American Fellows Program. All data and code to understand and assess the conclusions of this research are available in the main text, supplementary materials, and at the following repository: <http://dx.doi.org/10.15479/AT:ISTA:53>. T.B. and C.C.G. designed the experiments; T.B. and K.T. performed the experiments; A.M.C.A. and G.T. developed the model; A.M.C.A., T.B., G.T., K.T., and C.C.G. analyzed the data; A.M.C.A., E.B., and R.H. wrote analysis software and scripts; D.J.K. designed and manufactured microfluidic wafers; and A.M.C.A., T.B., G.T., and C.C.G. wrote the paper.

#### SUPPLEMENTARY MATERIALS

[www.sciencemag.org/content/356/6335/311/suppl/DC1](http://www.sciencemag.org/content/356/6335/311/suppl/DC1)  
 Materials and Methods  
 Figs. S1 to S19  
 Tables S1 to S11  
 Movies S1 to S3  
 References (26–37)

23 February 2016; resubmitted 30 September 2016  
 Accepted 13 March 2017  
 10.1126/science.aaf4762



**Biased partitioning of the multidrug efflux pump AcrAB-TolC underlies long-lived phenotypic heterogeneity**

Tobias Bergmiller, Anna M. C. Andersson, Kathrin Tomasek, Enrique Balleza, Daniel J. Kiviet, Robert Hauschild, Gasper Tkacik and Calin C. Guet (April 20, 2017)  
*Science* **356** (6335), 311-315. [doi: 10.1126/science.aaf4762]

Editor's Summary

**Drug efflux machinery inherited asymmetrically**

In dividing bacterial cells, asymmetric distribution of cell wall constituents occurs between mother cells and their progeny. Asymmetric distribution of efflux machinery in a growing population of bacterial cells results in heterogeneity in antibiotic resistance. One consequence is that in the presence of low levels of antibiotic, older cells tend to live longer than younger cells. Using a microfluidic device to trap and measure dividing cells, Bergmiller *et al.* showed that AcrAB-TolC, the main multidrug efflux pump of *Escherichia coli*, clusters at the pole of older cells (see the Perspective by Barrett *et al.*). As cell division proceeds and daughter cells age, they too gradually accumulate polar efflux pumps. *Science*, this issue p. 311; see also p. 247

---

This copy is for your personal, non-commercial use only.

---

**Article Tools** Visit the online version of this article to access the personalization and article tools:  
<http://science.sciencemag.org/content/356/6335/311>

**Permissions** Obtain information about reproducing this article:  
<http://www.sciencemag.org/about/permissions.dtl>

*Science* (print ISSN 0036-8075; online ISSN 1095-9203) is published weekly, except the last week in December, by the American Association for the Advancement of Science, 1200 New York Avenue NW, Washington, DC 20005. Copyright 2016 by the American Association for the Advancement of Science; all rights reserved. The title *Science* is a registered trademark of AAAS.